Asian Journal of Chemistry; Vol. 37, No. 10 (2025), 2415-2425
ASIAN JOURNAL OF CHEMISTRY
https://doi.org/10.14233/ajchem.2025.34338

Adsorption of Cd(II) and Cr(III) Ions using Magnetic Activated Carbon Derived from Plajau Wood (*Pentaspadon motleyi*)

MUHAMMAD YUSPRIYANNTO, NELLY WAHYUNI*, and ANIS SHOFIYANI

Department of Chemistry, Faculty of Mathematics and Natural Sciences, Tanjungpura University, Pontianak, Indonesia

*Corresponding author: Fax: +62 561 740185; Tel: +62 561 740185; E-mail: nellywahyuni@chemistry.untan.ac.id

Received: 25 June 2025 *Accepted*: 4 September 2025 *Published online*: 30 September 2025 AJC-22125

This study investigates the adsorption behaviour of Cd^{2+} and Cr^{3+} ions from aqueous solutions using magnetic activated carbon (MAC) synthesized from Plajau wood (*P. motleyi*). Magnetic activated carbon was synthesized by compositing activated carbon with magnetite (Fe_3O_4), using a Fe^{3+}/Fe^{2+} mixture in a 2:1 molar ratio. The formation of Fe_3O_4 on the carbon surface introduced new active sites and modified the pore structure of the activated carbon. Infrared spectra show the presence of magnetite in infrared absorption at 570 cm^{-1}, SEM-EDX analysis shows magnetite on the surface with oxide compound 6.8% and the XRD diffractogram confirms the suitability of magnetite. The optimum adsorption of Cd^{2+} and Cr^{3+} was achieved at pH 6 and 7, adsorbent doses of 0.04 g and 0.06 g, stirring speed of 150 rpm, contact times of 3 and 4 h and an initial concentration of 50 ppm, yielding maximum adsorption capacities of 48.36 mg/g and 39.27 mg/g, respectively. Adsorption of Cd^{2+} ion follows the Langmuir isotherm model (R^2 = 0.9123) and pseudo-second order kinetic model (R^2 = 0.9110). Meanwhile, the Cr^{3+} ion follows the Redlich-Peterson isotherm model (R^2 = 0.9475) and pseudo-second order kinetic model (R^2 = 0.9983). The efficiency of magnetic activated carbon recovery after adsorption was 81.18% indicating good magnetic responsiveness and potential for reuse with minimal material loss.

Keywords: Adsorption behaviour, Isotherms, Magnetite, Heavy metal ions, Plajau wood.

INTRODUCTION

Studies on adsorption properties using wood materials from plants have been widely studied. Several studies have explored wood materials as bioadsorbents including the adsorption of heavy metal ions using a composite of delignified and aminase wood powder [1], adsorption of hazardous dyes by activated carbon from wood fiber [2], adsorption of volatile organic compounds (VOCs) by activated carbon prepared from different types of wood materials [3] and adsorption of heavy metal ions using metal/polymer-doped wood powder [4,5].

Regenerating activated carbon is essential for reuse and cost-effectiveness. Common methods like heating and filtering can restore adsorption capacity but are time-consuming, energy-intensive, expensive and may cause carbon loss [6]. Another approach is to modify the adsorbent material using magnetic materials or materials that have magnetic properties [7,8]. Magnetite or Fe_3O_4 is an iron oxide phase that has the greatest magnetic properties among other phases (maghemite and hematite). The addition of Fe_3O_4 to activated carbon is a promising alternative to separate activated carbon from adsorbate solution faster and easier [9,10]. In addition, Fe_3O_4 can form new active sites or change the pore structure of the activated carbon surface so that the effective surface area can increase [11].

In past, magnetic activated carbon made from Kesambi wood (*Schleichera oleosa*) with magnetite was used to adsorb Cr(VI) ions. The process followed pseudo-second-order kinetics and Dubinin–Radushkevich isotherm, with a maximum capacity of 8.502 mg/g [12]. The resulting pore distribution is in the form of mesopores with a pore size of 4.55-7.01 nm. milarly, Nejadshafiee & Islami [13] perpared a magnetic activated carbon bioadsorbent from pistachio wood by incorporating Fe_3O_4 and immobilizing 1,4-butane sultone onto the carbon surface. The resulting material had a pore size of 30–50 nm (mesoporous to macroporous). It exhibited adsorption capacities of 147.05 mg/g for Pb^{2+} and 119.04 mg/g for Cd^{2+}, following the Langmuir isotherm model. However, activated carbon from carbon sources of various types of wood can produce pore structures and functional groups, which are not the

same, because each material has a different molecular weight and degree of polymerization. Wood with a high lignin constituent component has a density and hardness that can determine the structure and size of the pores. Plajau plant (*P. motleyi*) is an endemic plant belonging to the *anacardiaceae* group that grows on river banks or swamps and is found in the Ketapang Regency area, West Kalimantan. The height of the tree reaches 50 m, the branch-free trunk reaches 20 m and the trunk diameter reaches 70 cm. Plajau wood has good quality with a straight trunk shape, strong, hard and not easily cracked. Wood density is 480-800 Kg/m^3 with 15% moisture content [14].

Based on its density and hardness, Plajau wood exhibits high cellulose and lignin content, making it an excellent carbon source with inherent porosity and functional groups capable of metal adsorption. Furthermore, incorporating a magnetite composite enhances the surface area and facilitates easy separation for reuse. Thus, this study aims to characterize the magnetic activated carbon synthesized from plajau (*P. motleyi*) wood and investigate its adsorption performance for Cd^{2+} and Cr^{3+} ions. It seeks to determine the optimum adsorption conditions by varying pH, adsorbent mass, stirring speed, metal ion concentration and contact time. Furthermore, the study evaluates the adsorption isotherm and kinetics models based on the coefficient of determination (R^2) from the experimental data.

EXPERIMENTAL

The chemicals *viz*. iron(III) chloride hexahydrate ($FeCl_3 \cdot 6H_2O$), iron(II) sulfate heptahydrate ($FeSO_4 \cdot 7H_2O$), standard cadmium(II) solution (1000 mg/L) and standard chromium(III) solution (1000 mg/L), sodium hydroxide, silver nitrate and zinc chloride were of highest purity and procured from Merck, USA. The plajau wood was from obtained from the local garden at Ketapang city, West Kalimantan province, Indonesia and authenticated by the botanist.

Carbonization and physical-chemical activation: Plajau wood was ground into small pieces using a grinding machine and sun-dried. The dried material was carbonized in a pyrolysis tank at 250 ºC for 3 h. The resulting char was pulverized with a mortar and sieved through a 325-mesh sieve (≤ 45 µm). Physical activation was performed by calcining the carbon at 600 ºC for 1 h. For chemical activation, the carbon was mixed with 0.05 M $ZnCl_2$ solution, stirred and left covered for 24 h. The mixture was then filtered and the carbon washed with distilled water until free of chlorides (confirmed by $AgNO_3$ test), followed by drying in an oven at 100 ºC for 2 h.

Preparation of magnetic activated carbon (MAC): Magnetic activated carbon (MAC) was prepared by coprecipitation using a 2:1 molar ratio of $FeCl_3 \cdot 6H_2O$ (13.515 g) to $FeSO_4 \cdot 7H_2O$ (6.951 g), both dissolved in 200 mL of distilled water [9]. In other container, 40.932 g of activated carbon was dissolved in 200 mL of distilled water and stirred using a magnetic stirrer (70 ºC, 1 h). Then, added the metal solution slowly in the above activated carbon mixture. Finally, the magnetite-loaded activated carbon was dried at 65 ºC for 6 h, washed with distilled water until the water was clean and neutral and then separated using magnets.

Characterization: Moisture content, ash content, specific density and pass mesh 325 of MAC were determined according requirements of the Indonesian National Standard for activated charcoal (SNI 06-3730-1995). Activated carbon (AC) and magnetic activated carbon (MAC) were characterized using Fourier Transform Infrared Spectroscopy (FT-IR, Perkin-Elmer UATR Spectrum Two) to identify the functional groups in the 4000-400 cm^{-1} range. Surface area, pore volume and pore distribution were measured using a Surface Area Analyzer (SAA, Quantachrome TouchWin v1.22). X-ray diffraction (XRD, Bruker D2-Phaser) was employed to determine the crystal structure, while scanning electron microscopy coupled with energy dispersive X-ray spectroscopy (SEM-EDX, JEOL 6510A) was used to examine the surface morphology and elemental composition.

Determination of optimum adsorption conditions: The optimum adsorption of Cd^{2+} and Cr^{3+} ions was determined with pH variation (pH 2-8), adsorbent mass variation (0.02-0.1 g), rotation speed (100-200 rpm), contact time (30-240 min) and concentration of metal solution (30-70 ppm). Metal ions concentration were measured by atomic absorption spectrophotometer with three replicates. Adsorption data were analyzed according to isotherm models (Langmuir, Freundlich, Tempkin and Redlich Peterson) and adsorption kinetics (first-order, second-order, pseudo first-order and pseudo second-order kinetics models).

Collection of MAC from metal ion solution after adsorption: The separation of MAC from the metal ion solution after adsorption was used to determine the amount of adsorbent that could be withdrawn after adsorption of the metal solution. After adsorption of the metal solution at the optimum concentration is conducted, MAC in the solution is separated using a magnetic rod. Then the mass of magnetic activated carbon attached to the magnetic rod is dried, weighed and calculated as % adsorbent mass:

$$\text{Separated part} = \frac{A_2}{A_1} \times 100\% \quad (1)$$

where A_1 is the weight of MAC before adsorption and A_2 is the weight of MAC after separation.

Isotherm and kinetic models: Isotherm model and adsorption kinetics were evaluated with coefficient of determination (R^2) parameter and data error analysis. The error in the experiment was calculated as squared error (ErrSQ), absolute relative error (ARE), The hybrid fractional error function (HYBRID), marquadts percent squared deviation (MPSD) and absolute error (EABS) [15].

Calculation formula:

$$R^2 = 1 - \frac{\text{SS residual}}{\text{SS total}} \quad (2)$$

$$\text{ErrSQ} = \sum_{i=1}^{n} (Q_{e,i,calc} - Q_{e,i,exp})^2 \quad (3)$$

$$\text{ARE} = \sum_{i=1}^{n} \left(\frac{(Q_{e,i,exp} - Q_{e,i,calc})^2}{Q_{e,i,exp}} \right) \quad (4)$$

$$\text{HYBRID} = \sum_{i=1}^{n} \left(\frac{(Q_{e,i,calc} - Q_{e,i,exp})^2}{Q_{e,i,exp}} \right) \quad (5)$$

$$MPSD = \sqrt{\frac{1}{n-1}\sum_{i=1}^{n}\left(\frac{(Q_{e,i,exp} - Q_{e,i,calc})^2}{Q_{e,i,exp}}\right)} \quad (6)$$

$$EABS = \sum_{i=1}^{p} Q_{e,i,exp} - Q_{e,i,calc} \quad (7)$$

RESULTS AND DISCUSSION

The carbonization process obtained a carbon yield of 74.2% from Plajau wood. The percentage of mass lost indicates the amount of hemicellulose and partially decomposed cellulose. Some of the key factors affecting carbonization yield include the duration of heating and the temperature applied during the process. The use of the right heating time and heating temperature causes the carbon formation process to be more perfect. In this study, the pyrolysis time was 4 to 5 h with temperature reaching 270 ºC. Carbonization process triggers the decomposition of organic matter and will remove impurities in the raw material. Non-carbon elements are mostly lost in heating as well as the formation of pores or the opening of pores. Along with this process, there will be changes in the pore structure. Water evaporation occurs at 100-120 ºC, then the decomposition of cellulose into pyroglycan solution of wood gas and a little tar at 270-310 ºC, after which the decomposetion of lignin occurs so that more tar is produced while the pyroglycan solution and CO_2 gas decrease [9].

The primary objective of the activation process is to develop porosity and increase pore diameter by breaking hydrocarbon bonds or oxidizing surface compounds that may block the pores, thereby enhancing the surface area and improving the adsorption capacity of the carbon. Thus, in this work, carbon activation was performed through physical activation by heating the carbon in a furnace at 600 ºC for 30 min. Heating at this temperature facilitates the decomposition of lignin and contributes to the purification of the carbon [16]. The mass of carbon prior to activation was 141.14 g and after activation, it was reduced to 99.01 g, resulting in a yield of 70.15% from the physical activation process.

Carbon obtained from the physical activation process was further subjected to chemical activation using 0.05 M $ZnCl_2$, an acidic activating agent commonly employed to enhance the porosity and specific surface area [17]. The yield obtained from chemical activation was 94.19%. In another step, MAC was synthesized using $FeCl_3 \cdot 6H_2O$ and $FeSO_4 \cdot 7H_2O$ mixed with activated carbon at 70 ºC in an alkaline medium using NaOH solution. Fe_3O_4 precipitation was carried out at pH 8 to pH 11 with a Fe^{3+}/Fe^{2+} ratio of 2:1 in an alkaline medium. Mixing must be done carefully to prevent oxidized reactions that can lead to failure of magnetite formation. The oxidation reaction of Fe^{2+} by oxygen can produce $Fe(OH)_3$, while the oxidation of Fe_3O_4 can produce Fe_2O_3. One of the main advantages of magnetite-activated carbon (MAC) is its relatively rapid adsorption process; however, its limitations include the susceptibility of magnetite to oxidation and particle aggregation [18]. The conductivity value of the filtrate was tested with a conductometer and pH meter to obtain 40 µS and pH 7.

Characterization of MAC: MAC was characterized to determine the physico-chemical properties of the material produced. Analysis of moisture content, ash content and specific density was conducted according to SNI 06-3730-1995 Technical activated charcoal (Table-1).

FT-IR studies: The infrared spectra of the carbon sample showed an absorption band at a wave number of 3200 cm^{-1}. The absorption in the 3600-3200 cm^{-1} region is a stretching vibration of O-H or N-H. While the weak absorption band in the 900-700 cm^{-1} range is associated with aromatic C-H groups [18]. The absorption band at 1600 cm^{-1} is caused by C=C stretching vibrations on the aromatic ring. While the absorption band at 1200 cm^{-1} is caused by the aliphatic C-H stretch vibrations and C-H bending vibrations (Fig. 1) [19]. After the activation process, it was observed that the O-H stretching vibration band around 3200 cm^{-1} disappeared in the activated carbon due to the carbonization and activation accompanied by water loss (Fig. 1b). The absorption band at 1600-1400 cm^{-1} is caused by C=C stretching vibrations. While the absorption band at 1300-1100 cm^{-1} can be associated with aliphatic C-O stretching or phenol. The presence of hydroxyl groups, ethers, carbonyl groups, phenols and aromatic compounds confirm the structure of lignocellulose. The peak around 2600 cm^{-1} shows the -OH vibration of carboxylates [20]. On activated carbon, several absorption peaks also appear in the 900-000 cm^{-1} region showing C-H vibrations [21].

The infrared spectrum of MAC closely resembles that of activated carbon (Fig. 1c). The presence of absorption bands at 1600-1300 cm^{-1} appear is due to the C=C stretching vibrations as well as the presence of hydroxyl groups, ether, carbonyl groups at 1300-1100 cm^{-1} and C-H vibrations in the 800 cm^{-1} absorption band. The O-H vibrations around 3200 cm^{-1} were also appeared in the spectrum. The appearance of the new absorption peak at 570 cm^{-1} shows vibrations that may come from the metal oxide compounds. According to literature, the Fe–O vibrational bands appear in 750-500 cm^{-1} region, confirming the formation of Fe_3O_4 bonds during the magnetization process [10,13,20].

Moreover, the carboxyl and hydroxyl groups on the magnetic activated carbon are classified as hard bases; according to HSAB theory, this explains their interaction with metal ions on the adsorbent. Assuming that adsorption occurs mainly on active sites such as -COOH, -OH, then Cr^{3+} ions that have a greater possibility of interaction with these active groups will show a higher adsorption capacity [22,23].

TABLE-1
MOISTURE CONTENT, ASH CONTENT AND SPECIFIC DENSITY OF ACTIVATED CARBON (AC) AND MAGNETIC ACTIVATED CARBON (MAC)

Test parameters	AC (%)	MAC (%)	Quality requirements	Test method
Moisture content	7.06	6.37	Max. 15%	SNI 06-3730-1995 step 5.2
Ash content	2.46	2.46	Max. 10%	SNI 06-3730-1995 step 5.3
Density	0.35	0.31	0.30-0.35 g/mL	SNI 06-3730-1995 step 5.9
Pass mesh 325	95.66	92.76	Min. 90%	SNI 06-3730-1995 step 5.10

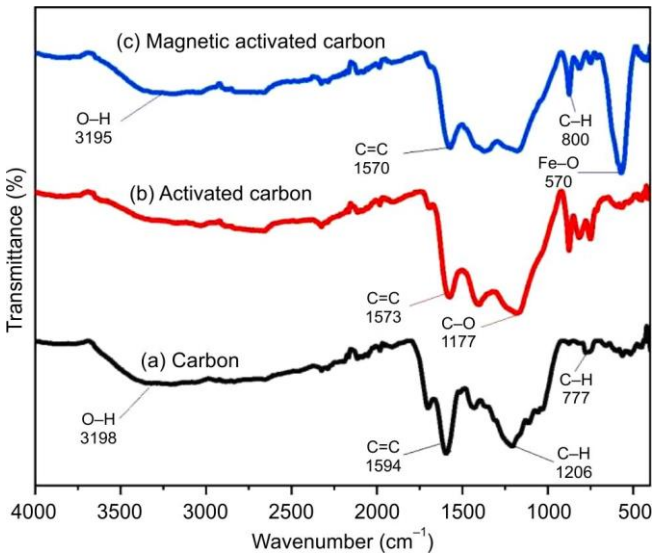

Fig. 1. FT-IR spectra of carbon, activated carbon and magnetic activated carbon

Morphological studies: Activated carbon with $ZnCl_2$ shows the presence of pores on the surface of the material. While the surface of magnetically activated carbon looks rougher and is accompanied by pores that facilitate the attachment of Fe_3O_4 particles around it. The addition of magnetite composites to activated carbon will cause the material to have a porous amorphous structure with a smooth surface but the surface is covered with distributed magnetic crystal particles [11]. While preparing the magnetic activated carbon, the iron oxide content must be optimized to enhance magnetic properties without clogging pores and reducing surface area. However, excess magnetic phase can clog pores, so its content must be optimized to the preserve magnetic properties while maintaining sufficient surface area [24].

Table-2 presents SEM-EDX analysis data for carbon (C), activated carbon (AC) and magnetic activated carbon (MAC), highlighting the composition of metal oxide compounds in each sample. The carbon content in all samples is significantly high, above 90%, indicating that the carbonation process of plajau wood was effective and produced carbon with high purity. Iron oxide was detected only in the MAC sample (6.80%), confirming the successful incorporation of magnetite into the activated carbon. Furthermore, the significantly higher carbon content compared to iron in the composite structure suggests that carbon remains the primary adsorptive component in the material [11].

TABLE-2
SEM-EDX OXIDE COMPOUND OF ADSORBENTS

Parameter	Oxide compound percentage (%)		
	Carbon	Activated carbon	Magnetic activated carbon
C	96.22	96.47	90.01
K_2O	0.39	Not detected	Not detected
Na_2O	Not detected	Not detected	0.25
CaO	0.84	0.73	0.51
CuO	0.98	0.79	0.71
ZnO	0.51	1.18	0.96
ZrO_2	1.07	0.82	0.76
FeO	Not detected	Not detected	6.80

Isotherm studies: Characterization of AC and MAC was carried out using the surface area analysis (SAA) instrument Quantachrome TouchWin v1.22, 40 pts isotherm. The purpose of this characterization is to determine the surface area, pore diameter and pore volume of AC and MAC samples produced from plajau wood. SAA analysis data for both materials are shown in Table-3. Based on the results of characterization conducted using multi-point Brunauer-Emmett-Teller (BET) measured by adsorption-desorption of nitrogen gas, the surface area of AC was 98.73 m^2/g and that of MAC was 152.23 m^2/g. The increase in surface area on MAC is due to the presence of Fe_3O_4 particles bound to the MAC structure and there are Fe_3O_4 particles covering the adsorbent surface (Fig. 2). Fe_3O_4 can form new active sites or change the pore structure of the AC surface so that the effective surface area increases. The same SEM image of the adsorbent surface characterization where there are Fe_3O_4 particles on the surface of AC. When Fe_3O_4 enters the pore, the effective surface area of AC will decrease. However, if the magnetite forms a thin layer that is evenly distributed and does not block access to the pores of the activated carbon, the effective surface area increases [11].

TABLE-3
CHARACTERIZATION RESULT BY
SURFACE AREA ANALYSIS

Parameter test	Activated carbon	Magnetic activated carbon
Surface area (m^2/g)	98.73	152.23
Pore volume (cc/g)	0.072	0.114
Pore size (nm)	1.453	1.496

The results showed that the average pore volume also increased where the activated carbon was 0.072 cc/g and the magnetic activated carbon increased to 0.114 cc/g. The pore volume increased with the presence of magnetite coating the activated carbon [25]. The pore size of activated carbon is obtained at 1.453 nm and for magnetic activated carbon at 1.496 nm, it does not change significantly so that the addition of composite compounds of iron oxide compounds does not enter the pores in the material so that it will not reduce its adsorption ability.

The porosity distribution of MAC studied using the Barrett-Joyner-Hanlenda (BJH) method shows the material with a specific surface area of 152.23 m^2/g has microporous category porosity (average pore size < 2 nm). Based on the results, it can be concluded that MAC from plajau wood has an average pore size in the micropore category since it has a pore size < 2 nm [26]. And in this study, Cr^{3+} and Cd^{2+} ions were used as adsorbates, with ionic radii of approximately 62 pm and 95 pm, respectively [27,28]. Based on their ionic radii, the adsorbates can theoretically enter and occupy the pores of the adsorbent, as their sizes are smaller than the pore diameter of the activated carbon. However, the adsorbent-adsorbate interaction in the adsorption of metal ions and magnetic activated carbon will follow the adsorption isotherm model according to the adsorption data.

XRD studies: The XRD diffraction patterns were analyzed in the 2θ angle range at 20º to 70º with a wavelength of 0.154 nm. The diffraction peaks that appear in the XRD pattern of carbon at an angle of 2θ are 24.34º, 35.92º and 38.18º, while

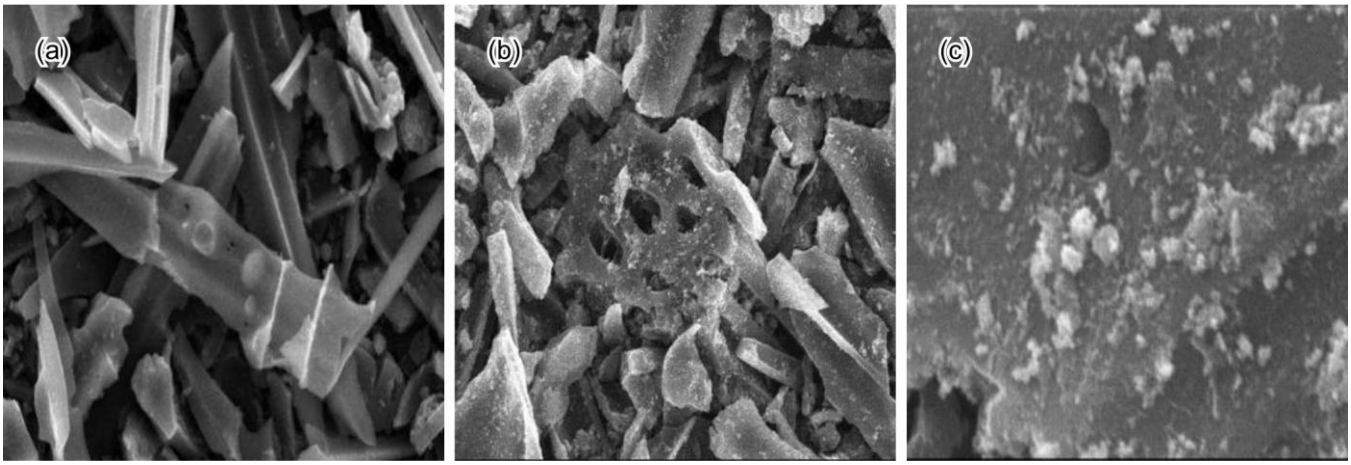

Fig. 2. SEM micrographs of magnetic activated carbon (a) 1000x (b) 10000x (c) 15000x

in activated carbon 26.62º, 29.28º, 35.89º, 39.25º and 43.06º. The occurrence of peaks in the 2θ = 23º-45º region indicates the presence of amorphous structures that are irregularly arranged on carbon, which are useful for producing gaps as adsorbents [11,29]. The diffractogram pattern of the MAC sample shows diffraction peaks at angles 2θ 30.06º, 35.41º, 43.05º, 56.96º and 62.41º (Fig. 3). This pattern corresponds to the cubic structure of magnetite particles on activated carbon with crystal planes (311), (400), (511) and (440) showing the crystal structure of iron oxide particles according to the standard data of iron oxide Joint Committee for Powder Diffraction Studies (JCPDS) Card No. 19-0629 [11]. The observed changes in the XRD diffraction pattern indicate alterations in the crystalline phase of activated carbon resulting from its compositing with magnetite. However, the interplanar spacing (*d*-spacing) at corresponding diffraction peaks remains unchanged, suggesting that while the phase composition is modified, the lattice parameters of the carbon structure are largely preserved. The diffraction pattern of MAC obtained has similarities with the results of previous research on the use of magnetite as an AC composite, namely MAC from pistachio wood [13] and Kesambi wood [12] and magnetite-composite of activated carbon [11].

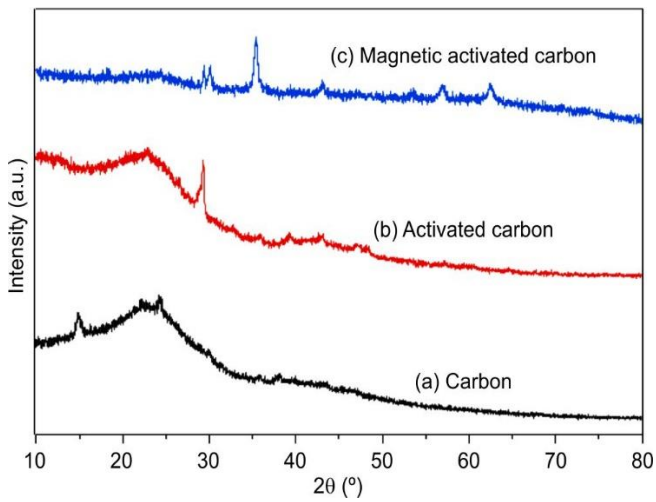

Fig. 3. Diffractogram of carbon, activated carbon and magnetic activated carbon

Adsorption of metal ions by MAC

Determination of adsorption optimum conditions: The effect of pH on metal ion adsorption was evaluated at pH levels of 3, 4, 5, 6, 7 and 8 for Cd^{2+} ions, and at pH levels of 2, 3, 4, 5, 6 and 7 for Cr^{3+} ions. Each uses a metal solution concentration of 50 mg/L with 0.1 g of magnetic activated carbon, stirring speed of 150 rpm and stirring time using an orbital shaker for 60 min. The observation results showing the effect of pH on the adsorption of Cd^{2+} and Cr^{3+} ions are shown in Fig. 4.

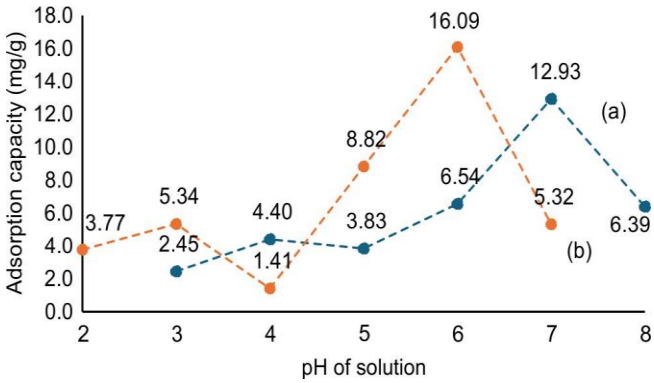

Fig. 4. Effect of pH on adsorption of (a) Cd^{2+} and (b) Cr^{3+} ions in solution

The degree of acidity (pH) is a critical factor in adsorption, as it influences the surface charge of the adsorbent and the speciation of metal ions in solution [30]. At low pH, metal ion adsorption is relatively low due to protonation of the adsorbent surface, which leads to competition from H^+ and H_3O^+ ions for active adsorption sites. Meanwhile, the metal ions in solution before being adsorbed by the adsorbent first undergo hydrolysis in water, producing protons as shown in the following equation:

$$M^{2+} + nH_2O \rightleftharpoons [M(OH)n^{2-n}]^+ + nH^+ \quad (8)$$

The hydroxo complex $[M(OH)n^{2-n}]^+$ resulting from the reaction will be more adsorbed than the free metal cation (M^{2+}). In acidic conditions, the above equation will shift to the left, so that the number of metal hydroxo complexes formed is less and the number of free metal cations is more.

At pH 6, the amount of Cd^{2+} ions adsorbed began to increase, namely 6.54 mg/g. The increase in the amount of metal ions adsorbed occurs up to pH 7. This shows that the adsorption of Cd^{2+} ions increases with changes in solution pH. Increasing the pH of the solution will be accompanied by decreasing the number of hydrogen ions and increasing the number of hydroxyl ions in the solution. The surface of the adsorbent will be negatively charged by releasing protons so that an attraction will occur leading to increased adsorption. This process facilitates adsorption of both metal ions through electrostatic attraction [31]; however, adsorption efficiency decreases at pH 8, reaching 6.39 mg/g. The decrease is likely due to the precipitation of Cd^{2+} ions in an alkaline atmosphere, so that adsorption does not occur optimally. In this study, the optimum pH for adsorption of Cd^{2+} ions were pH 7 with an adsorption capacity of 12.93 mg/g in 50 mg/L metal solution. The distribution of cadmium ion species in solution as a function of pH, where at acidic to neutral pH the species is in the form of Cd^{2+} and at pH 7 to alkaline atmosphere the species is in the form of $Cd(OH)^{+}$ and $Cd(OH)_2$ [32].

Adsorption of Cr^{3+} ions at acidic pH, namely pH 2 to pH 4, the adsorption capacity value is quite low at a maximum of 5.34 mg/g. At pH 5, the amount of Cr^{3+} metal adsorbed began to increase at 8.82 mg/g until it reached the optimum pH at pH 6 with an adsorbed percentage of 70.62%. As in the adsorption of Cd^{2+} ions, the low concentration of metal ions adsorbed at acidic pH is caused by protonation on the carbon surface. In addition, the species formed in solution are Cr^{3+} ions so that there is competition between protons and positive charges metal ions on the surface of activated carbon which causes the metal adsorption to be quite low. This is due to reduced competition between protons (H^{+}) and positively charged metal ions on the surface of activated carbon, so that metal ions can be easily absorbed in activated carbon [33]. At acidic pH up to pH 6 the species is in the form of Cr^{3+}, then changes in the form of $Cr(OH)_3$ species. This is in accordance with the optimum pH of Cr^{3+} ion adsorption obtained at pH 6 with adsorption capacity reaching 16.09 mg/g. Because at pH > 6, Cr^{3+} ions form hydroxide precipitates so that adsorption will not take place optimally.

Effect of adsorbent mass: The effect of adsorbent mass addition (Fig. 5) in metal ion adsorption was observed at various variations of adsorbent mass addition to 50 mg/L metal solution, *viz*. 0.02 g, 0.04 g, 0.06 g, 0.08 g and 0.1 g. The adsorption capacity was 44.64 mg/g. The measurement data showed adsorption of Cd^{2+} metal at 0.04 g adsorbent mass addition with adsorption capacity of 44.64 mg/g, while Cr^{3+} metal adsorption was optimum at 0.06 g adsorbent mass addition with adsorption efficiency reaching 39.82 mg/g.

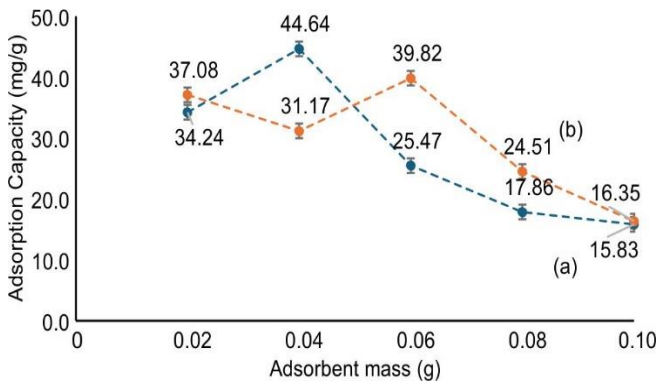

Fig. 5. Effect of adsorbent mass on adsorption of (a) Cd^{2+} and (b) Cr^{3+} ions

In the adsorption process, the amount of adsorbent mass has a significant effect on the efficiency and capacity of adsorption due to the interaction between the adsorbent and adsorbate molecules. In adsorption, the more adsorbent mass used, the maximum absorption rate will be and the smaller the adsorbent size, the wider the surface area will be [34]. The increase in adsorbent mass is accompanied by an increase in the number of particles and the surface area of activated carbon so that the number of places to bind metal ions increases and the adsorption efficiency increases. In this study, the addition of adsorbent mass decreased at the addition of 0.06 g for adsorption of Cd^{2+} ions and 0.08 g for Cr^{3+} ions. It is possible that the surface is close to saturation or saturation of the adsorbate, where the entire surface layer has bound the adsorbate or the diffusion of adsorbate that has not been bound back into solution [35].

Effect of stirring: The adsorption capacity of MAC for Cd^{2+} and Cr^{3+} ions was evaluated at different stirring speeds, with 150 rpm identified as the optimum condition. At this speed, Cd^{2+} achieved a maximum adsorption capacity of 61.20 mg/g, surpassing the capacities observed at 100 rpm and 120 rpm, indicating enhanced metal uptake with increased agitation. Similarly, Cr^{3+} adsorption capacity increased with stirring speed, reaching an optimum of 16.32 mg/g at 150 rpm.

The rotation speed of stirring can accelerate the adsorption process because the rotation speed helps the adsorbent to spread in all directions so that it can interact with the adsorbate thoroughly. With sufficiently vigorous stirring, the speed of adsorption can increase. Conversely, if the stirring is too slow, the adsorption process is slow as well. These results are in accordance with the effect of stirring speed where the higher the stirring speed, the greater the adsorption efficiency value, this is due to a large stirring speed causes higher contact between the adsorbent and the adsorbate, so that the adsorbent absorption can work optimally [36].

As the rotation speed increases, the particles of the material to be adsorbed come into contact with the activated carbon surface more frequently. This can increase the chance of interaction between pollutant molecules and the surface of activated carbon. Then at 170 rpm and 200 rpm, there is a decrease in adsorption capacity which is possible due to the stirring is too fast so that adsorption is less optimal. The rotation speed is too high, a phenomenon can occur where activated carbon particles move too fast so that they are not effective in absorbing adsorbates. In addition, excess kinetic energy can cause adsorbate particles to be released back from the activated carbon surface [37].

Effect of concentration: The effect of initial concentration on metal adsorption by MAC was observed using optimum conditions for certain adsorption condition parameters such as pH, adsorbent mass, rotation speed and contact time. Adsorption data of various metal concentrations are expressed in Fig. 6. The adsorption capacity is obtained from the amount of metal solution concentration adsorbed by the adsorbent

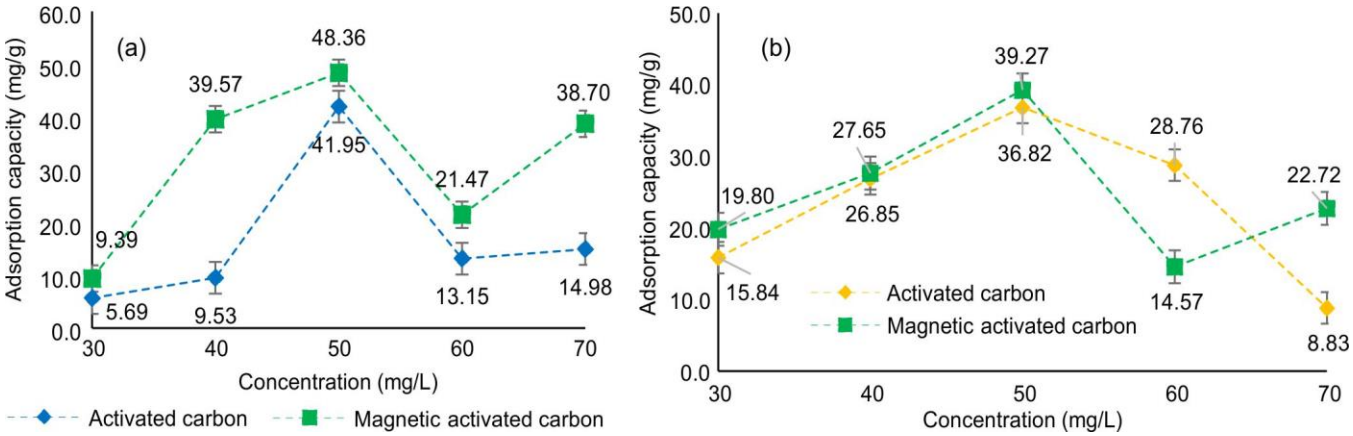

Fig. 6. Effect of concentration on the adsorption of (a) ion Cd^{2+} and (b) ion Cr^{3+} in solution

from several initial concentration variations of 30, 40, 50, 60 and 70 mg/L. It also shows the highest adsorption capacity of Cd^{2+} ions on AC was 41.95 mg/g, while on MAC it was 48.36 mg/g at a metal ion concentration of 50 mg/L. As for Cr^{3+} ions, the highest adsorption capacity on activated carbon was 36.83 mg/L, while on magnetic activated carbon it was 39.37 mg/L at a metal ion concentration of 50 mg/L. The difference in adsorption capacity of each sample is influenced by the surface area of the adsorbent. The greater the surface area of the sample, the higher the adsorption efficiency obtained. The increase in metal ion adsorption capacity on magnetic activated carbon can be concluded to be due to an increase in adsorbent surface area according to surface area analyzer (SAA) characterization data in Table-3.

Effect of contact time: One of the factors that also affect the adsorption process is the contact time between the adsorbent and the adsorbate. When the adsorption process takes place the adsorbent requires a certain time to interact with the adsorbate. Adsorption of metal ions was carried out using magnetic activated carbon with optimized parameters of pH, adsorbent mass, rotation speed and optimum concentration with variations in contact time given from 30 to 240 min. Fig. 7 shows the relationship between contact time and adsorption efficiency of ion Cd^{2+} and ion Cr^{3+} in solution. It can be seen that the contact time obtained from 50 mg/L Cd^{2+} ion solution contacted with 0.04 g adsorbent, 150 rpm at pH 7 is 180 min. While for Cr^{3+} ion 50 mg/L contacted with 0.06 g adsorbent, 150 rpm at pH 6 is 240 min (Table-4). Contact time is a very determining thing in the adsorption process where contact time is the length of time required for the adsorption of metal ions by magnetic activated carbon. Longer contact time allows the process of diffusion and attachment of adsorbate molecules to take place better, but under certain conditions it will stabilize because it is saturated so that saturation occurs where the active side of the adsorbent has experienced the maximum interaction.

The study on the selection of 2 (two) types of metal ions Cd^{2+} and Cr^{3+} as adsorbates based on the consideration of soft and hard properties according to Pearson's HSAB theory assumes that if the suitability of hard-soft acid-base properties and the presence of functional groups on the adsorbent become the dominant factors affecting the stability of adsorbent and adsorbate interactions, then the adsorption ability of

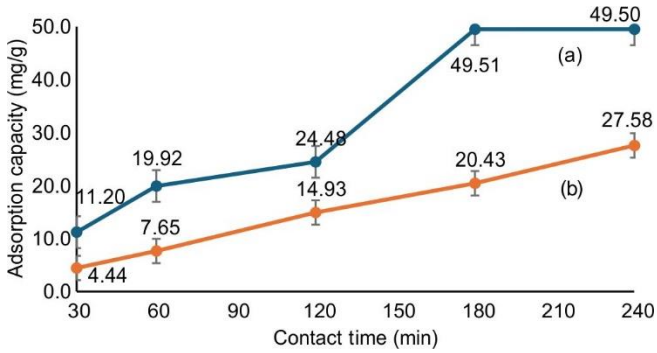

Fig. 7. Effect of contact time on adsorption of (a) Cd^{2+} and (b) Cr^{3+} ions

TABLE-4
OPTIMUM CONDITIONS OF ADSORPTION OF Cd^{2+} AND Cr^{3+} IONS WITH MAC

Test parameters	Adsorbate	
	Cd^{2+} ion	Cr^{3+} ion
pH	7	6
Adsorbent mass (g)	0.04	0.06
Rotation speed (rpm)	150	150
Concentration (mg/L)	50	50
Contact time (min)	180	240
Adsorption capacity (mg/g)	48.36 ± 4.27*	39.27 ± 0.88*
Adsorption efficiency (%)	79.28 ± 7.00*	87.64 ± 1.96*

*Values are expressed as mean ± standard deviation with n = 3.

Cr^{3+} ions as a hard metal with adsorbents will be higher than Cd^{2+} ions as a soft metal. Based on the adsorption data obtained, Cd^{2+} ions have a higher adsorption capacity of 48.36 mg/g than the adsorption capacity of Cr^{3+} ions, which is 39.27 mg/g. It can be concluded that the hard-soft nature of metal adsorption is not a determining factor in the interaction of adsorbent and adsorbate. Factors that can affect chemical adsorption are that there may be confounding ions that can affect adsorption. The greater the concentration of interfering ions with similar properties to the adsorbate, the greater the possibility of interference. Metal contamination in water containing a large number of coexisting ions, such as Na^+, K^+, Mg^{2+} and Al^{3+} will affect the migration of Cd^{2+} and Cr^{3+} ions on the adsorbent by binding to functional groups on the adsorbent surface and occupying active adsorption sites, thereby inhibiting the adsorption of Cd^{2+} and Cr^{3+} ions.

Adsorption isotherms: In this study, several adsorption isotherm models namely Langmuir, Freundlich, Tempkin and Redlich-Peterson were studied. Adsorption of Cd^{2+} ions using MAC in this study occurred physically chemically, but more likely to follow the Langmuir isotherm model with a coefficient of determination (R^2) of 0.9123. Based on the data obtained, the adsorption capacity of Cd^{2+} ions at a concentration of 50 mg/L is 48.36 mg/g with an adsorption efficiency of 79.28% (Table-5). The results indicate that 1 g of magnetic activated carbon can adsorb up to 48.36 mg of adsorbate at equilibrium. The Langmuir isotherm model assumes that the adsorbent has a finite number of homogeneous binding sites, each with equal affinity for adsorbate molecules. Adsorption occurs uniformly, with each site possessing the same activation energy and constant enthalpy. Moreover, the model assumes monolayer adsorption, where each binding site adsorbs only one molecule, resulting in a single adsorbate layer on the adsorbent surface [11].

The Langmuir isotherm model assumes a monolayer adsorption phenomenon, which means that one adsorbate molecule is adsorbed on the adsorbent surface and no other molecules are above it. The assumptions underlying the Langmuir isotherm such as homogeneous monolayer, equal energy and single component adsorption are potentially not always the case. Molecular modeling studies of adsorption revealed that the Langmuir framework is prone to failure in describing the adsorption data for multiscale porous materials since the adsorption capacity was found to be determined not only by chemical composition but also physically [38].

In the case of Cr^{3+} ions, adsorption tends to follow the Redlich-Peterson isotherm model, with a coefficient of determination (R^2) of 0.9475, which is higher than that of other isotherm models. Based on Table-5, the adsorption capacity of Cr^{3+} ions at a concentration of 50 mg/L was 39.27 mg/g with an adsorption efficiency of 82.17%. The Redlich-Peterson isotherm model combines the parameters of the Langmuir

TABLE-5
ADSORPTION ISOTHERM OF Cd^{2+} AND Cr^{3+} IONS WITH MAGNETIC ACTIVATED CARBON

Isotherm model	Formula	Reaction constant		Parameters	Value	
		Cd^{2+}	Cr^{3+}		Cd^{2+}	Cr^{3+}
Langmuir I	$C_e/Q_e = (1/b \cdot Q_m) + (C_e/Q_m)$	b = 0.0410 L/mg	b = 0.0587 L/mg	R^2	0.3783	0.9077
				ErrSQ	2.5530	0.7318
				ARE	0.9068	0.3080
				HYBRID	2.3426	0.3768
				MPSD	1.2087	0.1111
				EABS	2.8020	1.2477
Langmuir II	$1/Q_e = (1/b\ C_e)$	b = 0.7839 L/mg	b = 0.0797 L/mg	R^2	0.9123	0.1739
				ErrSQ	1.7933	0.0009
				ARE	0.6511	0.3093
				HYBRID	1.3084	0.0199
				MPSD	1.1408	0.1216
				EABS	2.6380	0.0628
Langmuir III	$Q_e/C_e = b \cdot Q_m - b \cdot Q_e$	b = 0.1132 L/mg	b = 0.1971 L/mg	R^2	0.6213	0.5755
				ErrSQ	7.7456	10.0685
				ARE	1.0372	1.3173
				HYBRID	0.7064	5.0871
				MPSD	1.5790	4.2515
				EABS	5.4340	5.2725
Freundlich	$\log Q_e = \log K_F + (1/n) \log C_e$	K_F = 0.3797 mg/g	K_F = 1.5751 mg/g	R^2	0.1752	0.2898
				ErrSQ	0.2774	0.4348
				ARE	0.1444	0.1778
				HYBRID	0.1983	0.2760
				MPSD	0.0471	0.0843
				EABS	0.8743	0.9900
Tempkin	$Q_e = B \ln A_T + B \ln C_e$	B = 319.20 J/mol A_T = 11.3158 L/mg	B = 4724 J/mol A_T = 11.3158 L/mg	R^2	0.2800	0.2800
				ErrSQ	713.198	713.1989
				ARE	0.5701	0.5701
				HYBRID	24.7995	24.7995
				MPSD	0.9795	0.9795
				EABS	47.2736	47.2736
Redlich-Peterson	$\ln (C_e/Q_e) = g \ln C_e - \ln K_R$	K_R = 23.4319 L/g g = 0.5342	K_R = 21.3216 L/g g = 0.8051	R^2	0.7371	0.9475
				ErrSQ	0.5695	0.2669
				ARE	0.0896	0.0962
				HYBRID	0.1737	0.1289
				MPSD	0.0111	0.0157
				EABS	1.4061	1.0165

Description: Q_e is the amount of adsorbate in the adsorbent at equilibrium, Q_m is a constant related to the single layer adsorption capacity, b is the Langmuir Constant, K_F: Freundlich constant, g is the heterogeneity index ($0 < g < 1$), K_R is the Redlich-Peterson constant.

and Freundlich equation models with hybrid adsorption mechanisms and does not follow ideal monolayer adsorption [38]. The Redlich-Peterson model is expressed in the equation:

$$\frac{\ln C_e}{Q_e} = g \ln C_e - \ln K_R \quad (9)$$

where K_R denotes the Redlich-Peterson constant (L/g) and g is the heterogeneity index between 1 and 0. This model has a linear relationship in concentration and an exponential function that can be simplified into a linear isotherm. If the value of g = 0, then it is simplified into the Henry isotherm equation, g < 1 into the Langmuir isotherm equation and g > 1 will be the Freundlich isotherm equation [39]. Based on the data analysis, the value of the parameter g in the Redlich-Peterson isotherm is 0.8051 (< 1), so the adsorption isotherm model of Cr^{3+} ions with magnetic activated carbon can also be assumed to be close to the Langmuir isotherm model.

Adsorption kinetics: In this study, adsorption kinetics were evaluated using four models *viz*. first-order, second-order, pseudo-first-order and pseudo-second-order. The results based on the adsorption data are presented in Table-6. The adsorption kinetics of Cd^{2+} and Cr^{3+} ions follow the pseudo-second order kinetics model since the correlation coefficient value for the pseudo-second order reaction kinetics is closer to 1 (with a correlation coefficient > 0.9) when compared to the correlation coefficient values of the other three kinetics models (Fig. 8). This indicates that there is a linear relationship between the variables involved, namely the variables t and t/q_t. This data shows that there is an increase in the value of t/q_t as t (adsorption time) progresses. The adsorption kinetics model was carried out by calculating the adsorption capacity of metal ions adsorbed by MAC (Q_t) using the equation below:

$$Q_t = \frac{C_o - C_e}{m} v \quad (10)$$

where m is the mass of adsorbent used (g) and v is the volume of metal ion solution (L). The pseudo-second order kinetic model (eqn. 11) can obtain the adsorption constant (k) from the linear regression equation with the function t/Q_t against t (time).

$$\frac{dQ_t}{t} = k(Q_e - Q_t)^2 \quad (11)$$

assuming that when the initial conditions (t = 0) no adsorption process has occurred (Q_t = 0), the following linear equation is obtained.

$$\frac{t}{Q_t} = \frac{1}{k.Q_e^2} + \frac{1}{Q_e} t \quad (12)$$

where k is the pseudo-second order model adsorption rate (g mg^{-1} min^{-1}). The adsorption rate constant value is an adsorption kinetics parameter that indicates how fast or slow the adsorption process takes place. The higher the k value, the faster the adsorption time [40]. The line equation for the adsorption of Cd^{2+} ions is y = 0.1958x + 6.2519. The reaction rate constant obtained is 0.0061 g mg^{-1} min^{-1}, which can be explained that 0.0061 g of adsorbate can be adsorbed on each

TABLE-6
ADSORPTION KINETICS OF Cd^{2+} AND Cr^{3+} IONS WITH MAGNETIC ACTIVATED CARBON

Kinetics model	Formula	Reaction constant		Parameters	Value	
		Cd^{2+}	Cr^{3+}		Cd^{2+}	Cr^{3+}
First order	$\ln C_e = -k \cdot t + \ln C_o$	k = 0.0064 mg L^{-1} min^{-1}	k = 0.0053 mg L^{-1} min^{-1}	R^2	0.8837	0.9715
				ErrSQ	0.1601	0.0245
				ARE	0.2257	0.1569
				HYBRID	0.1869	0.0758
				MPSD	0.0820	0.0512
				EABS	0.7096	0.3026
Second order	$1/C_e = k \cdot t + (1/C_o)$	k = 0.0003 mg L^{-1} min^{-1}	k = 0.0002 mg L^{-1} min^{-1}	R^2	0.8517	0.8944
				ErrSQ	0.0004	0.0002
				ARE	0.1821	0.1329
				HYBRID	0.0091	0.0044
				MPSD	0.0617	0.0221
				EABS	0.0368	0.0279
Pseudo-first order	$\log (Q_e - Q_t) = \ln Q_e - k \cdot t$	k = 0.0009 min^{-1}	k = -0.0003 min^{-1}	R^2	0.0025	0.5966
				ErrSQ	0.0946	0.1810
				ARE	0.0832	0.1615
				HYBRID	0.0645	0.1740
				MPSD	0.0105	0.0536
				EABS	0.5841	0.7630
Pseudo-second order	$t/Q_t = t/Q_e + (1/k \cdot Q_e^2) \log C_e$	k = 0.0061 g.mg^{-1} min^{-1}	k = 0.0096 g.mg^{-1} min^{-1}	R^2	0.9110	0.9983
				ErrSQ	2.0942	0.5953
				ARE	0.1264	0.0201
				HYBRID	3.0182	0.0380
				MPSD	0.0189	0.0005
				EABS	19.8681	1.3778

Description: k is the reaction rate constant

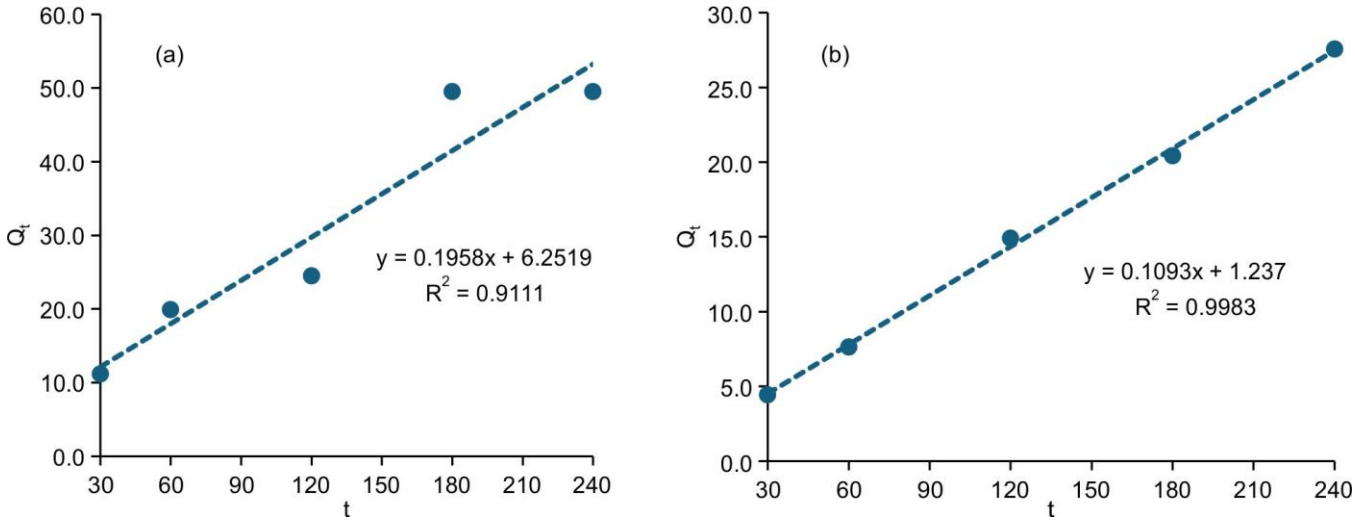

Fig. 8. Pseudo-second order kinetic model of (a) Cd^{2+} and (b) Cr^{3+} ions

mg of adsorbent when adsorption is carried out for 1 min. It can be interpreted that in 1 min of adsorption, there will be a transfer of 0.0061 g of metal solution for each mg of adsorbent surface. So, it can be concluded that adsorption that occurs according to pseudo-second order reaction kinetics illustrates that adsorption occurs on more than one active site on a straight adsorbent for pseudo-order second reaction kinetics.

Desorption studies: Collection of MAC from the metal ion solution after adsorption was carried out to determine the amount of adsorbent which could be withdrawn and collected again after adsorption of the metal solution. The experiment was conducted by pulling the MAC in the metal solution using a magnetic bar, then the adsorbent attached to the magnetic bar was dried using an oven and weighed. The mass of the collected adsorbent was compared with the mass of the initial adsorbent used before adsorption. The percentage of adsorbent mass obtained was 81.18%. Previous research conducted MAC separation using the same method, after adsorption was carried out and obtained a result of 87.0% [10]. This separation method by utilizing magnetic properties is easier to do for materials with small sizes (passing mesh 325) in solution. The results of this treatment can then be desorbed using a suitable desorption method and the adsorption ability of magnetic activated carbon can be tested again.

Conclusion

Based on this study, it can be concluded that the iron oxide (Fe_3O_4) in magnetic activated carbon (MAC) from Plajau wood is proven by infrared absorption at a wave number of 570 cm^{-1} and SEM-EDX analysis shows iron oxide compounds on the adsorbent surface with the composition is 6.8%. The XRD diffractogram pattern confirms the suitability of the standard data of iron oxide particles. The addition of magnetite composite is accompanied by an increase in the surface area and pore volume of the adsorbent. The optimum conditions for the adsorption of Cd^{2+} and Cr^{3+} ions with magnetic activated carbon are obtained at pH 6-7, adsorbent mass 0.04-0.06 g, stirring speed 150 rpm, contact time 3-4 h and optimum concentration 50 mg/L with adsorption capacities of 48.36 mg/g and 39.27 mg/g respectively. Adsorption of Cd^{2+} ions follows the Langmuir isotherm model ($R^2 = 0.9123$) and pseudo-second order kinetic model ($R^2 = 0.9110$). Meanwhile, the Cr^{3+} ions follow the Redlich Peterson isotherm model ($R^2 = 0.9475$) and pseudo-second order kinetic model ($R^2 = 0.9983$). The percentage mass of MAC was collected by magnetic bar after adsorption 81.18%.

CONFLICT OF INTEREST

The authors declare that there is no conflict of interests regarding the publication of this article.

REFERENCES

1. R. Del Sole, A.A. Fogel, V.A. Somin, G. Vasapollo and L. Mergola, *Materials*, **16**, 5322 (2023); https://doi.org/10.3390/ma16155322
2. X. Yang, H. Yi, X. Tang, S. Zhao, Z. Yang, Y. Ma, T. Feng and X. Cui, *J. Environ. Sci.*, **67**, 104 (2018); https://doi.org/10.1016/j.jes.2017.06.032
3. Y. Zhou, X. Liu, Y. Xiang, P. Wang, J. Zhang, F. Zhang, J. Wei, L. Luo, M. Lei and L. Tang, *Bioresour. Technol.*, **245**, 266 (2017); https://doi.org/10.1016/j.biortech.2017.08.178
4. S.J. Guo, X. Liu, M. Han, Y. Liu and S. Ji, *Cellulose*, **27**, 8155 (2020); https://doi.org/10.1007/s10570-020-03347-8
5. W. Jing, C. Yang, X. Lin, M. Tang, D. Lian, Y. Yu and D. Liu, *RSC Adv.*, **14**, 39995 (2024); https://doi.org/10.1039/D4RA06363
6. B. Verougstraete, M. Gholami, E. Pérez-Botella, M. Schoukens, T.R.C. Van Assche, Y.G. Rueda and J.F.M. Denayer, *Sep. Purif. Technol.*, **353C**, 128522 (2025); https://doi.org/10.1016/j.seppur.2024.128522
7. H.E. Reynel-Ávila, K.I. Camacho-Aguilar, A. Bonilla-Petriciolet, D.I. Mendoza-Castillo, H.A. González-Ponce and R. Trejo-Valencia, *Adsorpt. Sci. Technol.*, **2021**, 9917444 (2021); https://doi.org/10.1155/2021/9917444
8. Z. Shen, Y. Kuang, S. Zhou, J. Zheng, and G. Ouyang, *TrAC Trends Anal. Chem.*, **167**, 117241 (2023); https://doi.org/10.1016/j.trac.2023.117241
9. E.H. Alfiyani, N. Nurlina and N. Wahyuni, *Alchemy J.*, **18**, 130 (2022); https://doi.org/10.20961/alchemy.18.2.53647.130-139
10. W. Astuti, A. Trisyani, M. Biladudin, T. Sulistyaningsih and D. Prastiyanto, *IOP Conf. Ser. Earth Environ. Sci.*, **700**, 012043 (2021); https://doi.org/10.1088/1755-1315/700/1/012043
11. E. Mirzaee and M. Sartaj, *J. Hazardous Mater. Adv.*, **6**, 100083 (2022); https://doi.org/10.1016/j.hazadv.2022.100083

12. Y. A.B. Neolaka, Y. Lawa, J. Naat, Y.E. Lindu, H. Darmokoesoemo, A.A.P. Riwu, B.A. Widyaningrum, M. Iqbal and H.S. Kusuma, *React. Funct. Polym.*, **166**, 105000 (2021); https://doi.org/10.1016/j.react functpolym.2021.105000
13. V. Nejadshafiee and M.R. Islami, *Mater. Sci. Eng. C*, **101**, 42 (2019); https://doi.org/10.1016/j.msec.2019.03.081
14. Z. Sudarmono and Dodo, *Proc. Indon. Biodiver. Soc. Semester Meet.*, **1**, 602 (2015); https://doi.org/10.13057/psnmbi/m010337
15. R. Nofiani, Rio, K. Komalasari, P. Ardiningsih and S.J. Santosa, *Sains Malays.*, **51**, 1753 (2022); https://doi.org/10.17576/jsm-2022-5106-12
16. V. Poursorkhabi, M.A. Abdelwahab, M. Misra, B. Gharabaghi, H. Khalil and A.K. Mohanty, *Front. Energy Res.*, **8**, 208 (2020); https://doi.org/10.3389/fenrg.2020.00208
17. J. Lou, X. Xu, Y. Gao, D. Zheng, J. Wang and Z. Li, *RSC Adv.*, **6**, 112166 (2016); https://doi.org/10.1039/C6RA24397E
18. S. Rodríguez-Sánchez, B. Ruiz, D. Martínez-Blanco, M. Sánchez-Arenillas, M.A. Diez, J.F. Marco, P. Gorria and E. Fuente, *Appl. Surf. Sci.*, **551**, 149407 (2021); https://doi.org/10.1016/j.apsusc.2021.149407
19. A.H. Pinto, J.K. Taylor, R. Chandradat, E. Lam, Y. Liu, A.C.W. Leung, M. Keating and R. Sunasee, *J. Environ. Chem. Eng.*, **8**, 104187 (2020); https://doi.org/10.1016/j.jece.2020.104187
20. H.K. Yagmur and İ. Kaya, *J. Mol. Struct.*, **1232**, 130071 (2021); https://doi.org/10.1016/j.molstruc.2021.130071
21. Z. Zhang, T. Wang, H. Zhang, Y. Liu and B. Xing, *Sci. Total Environ.*, **757**, 143910 (2021); https://doi.org/10.1016/j.scitotenv.2020.143910
22. A.A. Alluhaybi, A. Alharbi, A.M. Hameed, A.A. Gouda, F.S. Hassen, H.S. El-Gendy, B.M. Atia, A.R. Salem, M.A. Gado, A. Ene, H.A. Awad and H.M.H. Zakaly, *Molecules*, **27**, 5087 (2022); https://doi.org/10.3390/molecules27165087
23. C.M. Simonescu, V. Lavric, A. Musina, O.M. Antonescu, D.C. Culita, V. Marinescu, C. Tardei, O. Oprea and A.M. Pandele, *J. Mol. Liq.*, **307**, 112973 (2020); https://doi.org/10.1016/j.molliq.2020.112973
24. B. Liu, C. Du, J.J. Chen, J.Y. Zhai, Y. Wang and H.L. Li, *Chem. Phys. Lett.*, **771**, 138535 (2021); https://doi.org/10.1016/j.cplett.2021.138535
25. A.S. Zulaicha, Buhani and Suharso, *J. Phys. Conf. Ser.*, **1751**, 012086 (2021); https://doi.org/10.1088/1742-6596/1751/1/012086
26. Y.A.B. Neolaka, A.A.P. Riwu, U.O. Aigbe, K.E. Ukhurebor, R.B. Onyancha, H. Darmokoesoemo and H.S. Kusuma, *Results Chem.*, **5**, 100711 (2023); https://doi.org/10.1016/j.rechem.2022.100711
27. Q. Lin, Q. Wang, M. Liao, M. Xiong, X. Feng, X. Zhang, H. Dong, D. Zhu, F. Wu and Z. Mu, *ACS Appl. Mater. Interfaces*, **13**, 18274 (2021); https://doi.org/10.1021/acsami.1c01417
28. H. Ghorbani, M. Eshraghi and A.A.S. Dodaran, *Physica B*, **634**, 413816 (2022); https://doi.org/10.1016/j.physb.2022.413816
29. R. Dungani, S.S. Munawar, T. Karliati, J. Malik, P. Aditiawati and Sulistyono, *J. Korean Wood Sci. Technol.*, **50**, 256 (2022); https://doi.org/10.5658/WOOD.2022.50.4.256
30. D. Gu, Y. Zhu, Z. Xu, N. Wang and C. Zhang, *J. Adv. Mater. Phys. Chem.*, **4**, 187 (2014); https://doi.org/10.4236/ampc.2014.410022
31. R. Aziam, M. Chiban, H. Eddaoudi, A. Soudani, M. Zerbet and F. Sinan, *Eur. Phys. J. Spec. Top.*, **226**, 977 (2017); https://doi.org/10.1140/epjst/e2016-60256-x
32. O.A. Oyetade, V.O. Nyamori, S.B. Jonnalagadda and B.S. Martincigh, *Desalination Water Treat.*, **108**, 253 (2018); https://doi.org/10.5004/dwt.2018.21955
33. M.A. Abu-Daabes, E.A. Zeitoun and W. Mazi, *Water*, **15**, 1070 (2023); https://doi.org/10.3390/w15061070
34. M. Zhang, W. Wang, Z. Lv and S. Wang, *Environ. Sci. Pollut. Res. Int.*, **30**, 11926 (2023); https://doi.org/10.1007/s11356-022-22961-6
35. G.B. Adebayo, H.I. Adegoke and S. Fauzeeyat, *Appl. Water Sci.*, **10**, 213 (2020); https://doi.org/10.1007/s13201-020-01295-z
36. K. Kuśmierek and A. Świątkowski, *React. Kinet. Mech. Cat.*, **116**, 261 (2015); https://doi.org/10.1007/s11144-015-0889-1
37. Z. Yi, J. Yao, M. Zhu, H. Chen, F. Wang and X. Liu, *SpringerPlus*, **5**, 1160 (2016); https://doi.org/10.1186/s40064-016-2839-4
38. S. Alafnan, A. Awotunde, G. Glatz, S. Adjei, I. Alrumaih and A. Gowida, *J. Petrol. Sci. Eng.*, **207**, 109172 (2021); https://doi.org/10.1016/j.petrol.2021.109172
39. T.A. Nugroho, C.A. Riyanto and N.R. Aminu, *Indones. J. Chem. Anal.*, **7**, 12 (2024); https://doi.org/10.20885/ijca.vol7.iss1.art2
40. Livia, W.B. Kurniawan and H. Aldila, *Indones. J. Phys. Res.*, **2**, 31 (2022); https://doi.org/10.33019/jrfi.v2i2.3221